Effects of prefreezing on the drying characteristics, structural formation and mechanical properties of microwave-vacuum dried apple

Effects of Prefreezing on the Drying Characteristics, Structural Formation and Mechanical Properties of Microwave-vacuum Dried Apple

Yasumasa ANDO [a,*], Shoji HAGIWARA [b], Hiroshi NABETANI [b,c], Itaru SOTOME [c], Tomoya OKUNISHI [b], Hiroshi OKADOME [b], Takahiro ORIKASA [d,e], Akio TAGAWA [f]

[a] *Institute of Vegetable and Floriculture Science, NARO, 360 Kusawa, Anou, Tsu, Mie 514-2392, Japan.*

[b] *Food Research Institute, NARO, 2-1-12 Kannondai, Tsukuba, Ibaraki 305-8642, Japan.*

[c] *Graduate School of Agricultural and Life Sciences, The University of Tokyo, 1-1-1 Yayoi, Bunkyo-ku, Tokyo 113-8657, Japan.*

[d] *Faculty of Agriculture, Iwate University, 3-18-8 Ueda, Morioka, Iwate 020-8550, Japan.*

[e] *Agri-Innovation Center, Iwate University, 3-18-8 Ueda, Morioka, Iwate 020-8550, Japan.*

[f] *Professor Emeritus, Graduate School of Horticulture, Chiba University, 648 Matsudo, Matsudo, Chiba 271-8510, Japan.*

Corresponding author: Yasumasa Ando, *Institute of Vegetable and Floriculture Science, NARO, 360 Kusawa, Anou, Tsu, Mie 514-2392, Japan.*

E-mail yaando@affrc.go.jp

Tel +81-50-3533-4628

Abstract

The effects of prefreezing on the drying rate, internal structure and mechanical properties of apple fruit processed by microwave-vacuum drying (MVD) were evaluated. The drying rate of the prefrozen sample was approximately 1.2 to 1.3 times higher than that of the nontreated sample. In the frozen-thawed tissue, damage to the cell wall structure and cell membrane due to ice crystal formation during freezing was confirmed; thus, improvement in the drying rate was suggested to be the result of accelerated water transfer in the tissue. Structural observation using X-ray computed tomography showed that the prefrozen MVD sample had a porous internal structure with larger voids than air dried or nonpretreated samples. Alterations in the mechanical properties, such as higher maximum stress and number of peaks during the puncture test, indicating a softer and crisper texture, were observed in the prefrozen MVD sample.

Keywords: Microwave-vacuum drying, Prefreezing, Apple, Drying rate, X-ray CT, Mechanical property

Nomenclature

C_m	capacitance of cell membrane (F)
E	elastic modulus (Pa)
j	imaginary unit (–)
k	drying rate constant (h^{-1})
M	moisture content (–)
M_e	equilibrium moisture content (–)
M_0	initial moisture content (–)
P	constant phase element exponent (–)
R_i	intracellular fluid resistance (Ω)
R_e	extracellular fluid resistance (Ω)
R^2	determination coefficient (–)
t	drying time (h)
T	constant phase element coefficient ($F \cdot s^{(P-1)}$)
Z	complex impedance (Ω)
Z_b	combined impedance of the model (b) (Ω)
Z_{CPE}	impedance of constant phase element (Ω)
θ	phase angle (rad)
σ	stress (Pa)
σ_{max}	maximum stress (Pa)
ω	angular frequency ($rad \cdot s^{-1}$)

1. Introduction

Drying is one of the most classical processing methods for fruit and vegetables, resulting in an extended shelf-life, lighter weight for transportation, and reduced space requirements for storage (Dandamrongrak et al., 2002). Although dried fruit and vegetables have been commonly manufactured by relatively simple drying methods such as sun drying and air drying, newer drying techniques have been developed to reduce the drying time, as well as to improve the energy efficiency and quality of dried fruit and vegetables (Sagar and Suresh, 2010).

Microwave-vacuum drying (MVD) is a relatively newly developed drying technique in which water evaporation progresses rapidly because of the rapid heating of the food material, caused by the action of the microwave energy absorbed by the material in a high-frequency electric field on the water molecules in the material, and the low boiling temperature of water in the reduced-pressure environment. Application of MVD to fruit and vegetables such as cranberry (Zielinska et al., 2017a; Zielinska et al., 2017b; Yongsawatdigul and Gunasekaran, 1996), blueberry (Zielinska and Markowski, 2016; Zielinska and Michalska, 2016; Zielinska et al., 2015), banana (Jiang et al., 2014; Drouzas and Schubert, 1996), potato (Bondaruk et al., 2007), durian (Bai-Ngew et al., 2011), tomato (Orikasa et al., 2018; Abano et al., 2012; Durance and Wang, 2002), mango (Pu and Sun, 2014), carrot (Nahimana and Zhang, 2011; Stępień, 2008; Cui et al., 2004; Lin et al., 1998) and apple (Chong et al., 2014; Huang et al., 2012) has been studied. It was shown that MVD has a higher drying rate (Zielinska et al., 2016; Giri and Prasad, 2007; Bondaruk et al., 2007; Durance et al., 2002; Lin et al., 1998) and

85 consumes less energy (Jiang, et al., 2017; Durance et al., 2002) than conventional air
86 drying. Moreover, the porous structure of the dried materials allows for a high
87 rehydration rate (Therdthai and Zhou, 2009; Giri et al., 2007; Durance et al., 2002; Lin
88 et al., 1998) and has a different texture (Zielinska, et al., 2016; Bondaruk et al., 2007)
89 compared to materials dried by other methods. There is also less deterioration of
90 constituents such as ascorbic acid (Hu et al., 2006; Lin et al., 1998), carotenoids (Cui et
91 al., 2004), chlorophyll (Hu et al., 2006; Yanyang et al., 2004; Cui, et al., 2004) owing to
92 the prevention of excessive increases in temperature and oxidation due to the presence
93 of air.

94 In some studies related to the drying of fruit and vegetables, the effect of
95 pretreatment on the drying rate has been reported. It has been shown that
96 freezing/thawing pretreatment, in particular, can effectively increase the drying rate
97 (Dandamrongrak et al., 2002; Eshtiaghi et al., 1994). The increase in drying rate has
98 been attributed to changes in the permeability of the cell membrane and damage of the
99 cell wall structure of the sample tissue during freezing (Ando et al., 2016; Nieto et al.,
100 1998; Alvarez et al., 1995). Zielinska et al. (2015) examined the effect of
101 freezing/thawing pretreatment in the MVD of blueberries, and reported that the
102 application of prefreezing could effectively reduce the drying time and the associated
103 specific energy consumption.

104 The objectives of this study were to investigate the effects of the prefreezing on
105 the MVD characteristics and post-drying structural and mechanical properties of the
106 apple fruit, which is a popular material consumed as a dried product, and to compare the

quality attributes to the conventional hot-air dried sample to clarify the effectiveness of the prefreezing-MVD combination.

2. Materials and methods

2.1 Sample preparation

Apples (*Malus pumila* var. *domestica* cv. Fuji) were obtained from a local market and stored in a refrigerator at 5 °C prior to the experiments (within one week). The initial moisture content of the samples was gravimetrically determined according to the standard method (The Council for Science and Technology, MEXT, Japan, 2005). Briefly, the fresh sample was milled and mixed with a drying aid (Celite No.503; Imerys Filtration Minerals Inc., San Jose, USA). The aluminum cup containing the mixture was placed on a hot water bath controlled at 70 °C to predry the mixture, then the mixture was completely dried in a vacuum chamber (3606; Labline Instruments Inc., Melrose Park, USA) at a set temperature of 70 °C for 5 h. The initial moisture content of the fresh samples was 5.377±0.017 and 5.387±0.022 on a dry basis (g-water/g-dry) for 2 lots obtained on different days, from an average of 8 samples for each lot.

Apples were peeled and cut into a quarter-circle shape with 10 mm thickness and 30 mm radius. The sample temperature was conditioned in an incubator (CN-25C; Mitsubishi Electric Engineering Ltd., Tokyo, Japan) at 25 °C for 1 h before drying. The sample was frozen in a freezer (HRF-90XT; Hoshizaki Corp., Aichi, Japan) at –20 °C, and stored for 6 days to 2 weeks until use for the experiment. The frozen sample was

129 thawed in the incubator at 25 °C for 3 h and used as the prefrozen-thawed sample. It
130 was confirmed that the temperature of both nontreated and prefrozen-thawed samples
131 reached approximately 25 °C before drying.
132
133 *2.2 Drying procedure and calculation of drying rate*
134 Figure 1 shows the configuration of the apparatus for MVD. In the MVD
135 experiment, a glass desiccator was placed in a microwave oven (MOH-3000; Micro
136 Denshi, Saitama, Japan), and the inside of the desiccator was depressurized using a
137 vacuum pump (G-50DA; Ulvac Kiko Inc., Kanagawa, Japan). The actual microwave
138 power output of the oven was measured by following the method of Japanese Industrial
139 Standard (JIS) C9250: 2007 at the maximum power of 3 kW and was determined to be
140 2.58 kW. The evaporated moisture during sample drying was collected using a cold trap
141 (CA301; Yamato Scientific Co., Ltd., Tokyo, Japan). The pressure in the desiccator was
142 maintained at 1.5 kPa during drying using a pressure regulation unit (NVC-2300B;
143 EYELA, Tokyo, Japan). Eight apple samples (55.03 ± 6.03 g-fresh weight) were placed
144 in the desiccator, and the output power of the microwave at 2450 MHz (frequency at
145 which most commercial microwave operates) was controlled at 200, 300 or 400 W
146 (3.63, 5.45, 7.27 W/g-fresh weight). The microwave was intermittently irradiated at a
147 cycle of 1 min irradiation and 1 min pause to prevent the excess increase of sample
148 temperature. The central temperature of the sample during MVD was measured using a
149 fiber optic thermometer (FL-2000; Anritsu Meter Co., Ltd., Tokyo, Japan) with a fiber
150 probe.

151 For air drying (AD), samples were placed in a drying chamber (DN-42; Yamato
152 Scientific Co., Ltd.) at a controlled temperature of 40, 60 and 80 °C. The air velocity in
153 the chamber was 1.5 ± 0.1 $m \cdot s^{-1}$ on average during continuous measurement over 3
154 min. The central temperature of the sample during AD was measured using a T-type
155 thermocouple with a wire diameter of 0.34 mm.
156 After specified drying times, the samples were removed from the drying
157 apparatus and weighed. The moisture content was calculated from both the initial
158 moisture content and the mass. The samples were dried until the moisture content
159 reached below 0.2 g-water/g-dry. Based on this period, the drying rate of the samples
160 was estimated using the exponential model which stands for the first-order reaction,
161 incorporating a single drying rate constant for the combined effect of the various
162 transport phenomena (Babalis et al., 2006; Orikasa et al., 2008):

(1)

163 $$\frac{M-M_e}{M_0-M_e}=\exp(-kt)\ ,$$

164 where M, M_e and M_0 denote the moisture content, the equilibrium moisture content and
165 the initial moisture content respectively, k denotes the drying rate constant (h^{-1}) and t
166 denotes the drying time (h). In this study, the constants k and M_e were estimated by
167 using the method of least squares. After each drying, samples were dried in a
168 thermostatic chamber at 60 °C for 12 h to remove any residual moisture and equalize
169 the moisture condition before the evaluation of dried sample explained below.
170
171 *2.3 Evaluation of cell membrane damage in the sample tissue*
172 The cell membrane within the plant tissue controls the migration of moisture

173 into cells, and structural damage affects the moisture migration rate during drying
174 processing (Vaccarezza et al., 1974). In the present study, therefore, structural damage
175 of the cell membrane of the prefrozen sample tissue was evaluated by electrical
176 impedance spectroscopy, which has been widely used to estimate the physiological
177 status of various biological tissues (Zhang and Willison, 1992a, 1992b; Ando et al.,
178 2014; Imaizumi et al., 2015; Watanabe et al., 2017).

179 Stainless steel needle electrodes spaced 10 mm apart were inserted into the
180 sample tissue to a depth of 5 mm, then the impedance magnitude $|Z|$ (Ω) and phase
181 difference θ (rad) of the samples before and after freeze-thawing at a frequency range
182 from 50 Hz to 500 kHz were measured using an impedance analyzer (E4990A;
183 Keysight Technologies, Santa Rosa, USA). The measurements were replicated 15–16
184 times for each sample. The test was carried out at a room temperature of 25 °C.

185 The measured data were analyzed with an equivalent circuit model of cellular
186 tissue shown in Fig. 2. Figure 2a shows a biological cell model that takes into account
187 the capacitance of the cell membrane, C_m, and resistances of intra- and extra-cellular
188 fluids, R_i and R_e. The model (b) shown in Fig. 2b is modified by substituting a constant
189 phase element (CPE) for C_m in model (a) to fit the impedance characteristics of the
190 biological tissue consisting of electrically inhomogeneous multiple cells, which
191 produces a time constant distribution. The impedance of CPE (Z_{CPE}) is shown as:

192 $$Z_{CPE}=\frac{1}{(j\omega)^P T}, \tag{2}$$

193 where ω denotes the angular frequency (rad·s^{-1}), T denotes the CPE coefficient and P
194 denotes the CPE exponent ($0 \le P \le 1$). The combined impedance of the model (b) is

represented by the following equation:

$$Z_b = \frac{R_e(Z_{CPE}+R_i)}{R_e+Z_{CPE}+R_i} .$$

The measured impedance data were fitted to Eq. 3 using complex nonlinear least squares curve fitting (Macdonald, 1992) and each circuit parameter was determined.(3) The determination coefficient, R^2, was calculated as follows to evaluate the goodness of fit of the model (Imaizumi et al., 2015):

$$R^2 = 1 - \frac{\sum_i \left(|Z_i| - |\hat{Z}_i| \right)^2}{\sum_i \left(|Z_i| - |\overline{Z}| \right)^2} , \quad (4)$$

where $\hat{Z}$ denotes the approximate value of Z, and $\overline{Z}$ denotes the average value of Z. Here, CPE constant T was converted to apparent capacitance C using the equation below (Ando et al., 2014; Hsu and Mansfeld, 2001):

$$C = T^{\frac{1}{P}} (R_e+R_i)^{\frac{1-P}{P}} . \quad (5)$$

In this study, apparent capacitance C, obtained from Eq. 5, was defined as the cell membrane capacitance, C_m (Ando et al., 2014). The detailed procedure of the equivalent circuit analysis was described in the literature (Ando et al., 2017).

2.4 Microscopic observation of the sample tissue

The flesh tissue cut from the fresh and frozen samples before drying was fixed in a FAA solution (37 % formaldehyde: acetic acid: 50 % ethanol solution, 5: 5: 90 v/v) for 2 days, then dehydrated through a graded ethanol series (50, 70, 80, 90, 95 and 100 %). The dehydrated samples were embedded in methacrylate resin (Technovit 7100; Heraeus Kulzer GmbH, Wehrheim, Germany), and sectioned into 4-μm thick slices

using a microtome (RM2145; Leica, Wetzlar, Germany). The sections were stained with safranine (Wako, Osaka Japan) and Fast green FCF (Wako, Osaka Japan) solutions, and observed with an optical microscope (DM LB; Leica) equipped with a digital camera (α5100; Sony, Tokyo, Japan).

2.5 Visualization of the internal structure of the dried sample

A micro focus X-ray computed tomography (X-ray CT) system (SMX-100CT; Shimadzu Corp., Kyoto, Japan) was used for the observation of both the whole structure and microstructure of the dried samples. The dried samples were scanned using the X-ray CT system at an X-ray tube voltage of 70 kV and current of 40 μA. For observation of the microstructure, the center part of the dried sample was cut with a sharp knife into a small block (3 mm × 3 mm × 6 mm), and scanned at a voltage of 50 kV and current of 40 mA. For both observations, 1200 transmission images were obtained through 360 degree rotation. The tomographic images of the dried sample were reconstructed using software (Exfact VR; Nihon Visual Science Inc., Tokyo, Japan).

2.6 Mechanical properties of the dried sample

A universal testing machine (5542; Instron, Norwood, USA) equipped with a 500 N load cell was used for the puncture test of dried samples. The dried sample was placed on a metal base with a 10 mm diameter hole in the center, then a cylindrical plunger 3.2 mm in diameter was inserted at a speed of 1 $mm \cdot s^{-1}$ into the center flat surface of the sample until the plunger passed through the center of the hole and

completely penetrated the sample. The trigger load was set to 0.05 N. The thickness at the center flat part of the sample was measured using a caliper.

The value of stress σ was calculated by dividing the measured force with the cross-sectional area of the plunger, and the strain was calculated by dividing the displacement with the thickness of the punctured part of the sample. Maximum stress σ_{max} (Pa), elastic modulus E (Pa), and number of peaks were calculated as indices of the mechanical properties. The value of E was defined as the slope of the first linear part of the stress-strain curve. The number of peaks refers to the number of positive peaks greater than a threshold force counted on the force-deformation curve, and has been used as one of the indices of the crispness of dry material (Dogan and Kokini, 2007). The value of the threshold was set at 0.044 N, equivalent to 15 % of the average drop off force value of all tested samples (Dogan and Kokini, 2007). The number of peaks were calculated only for the prefrozen AD and MVD samples in order to compare their crispness. The experiments were replicated 16–18 times for each sample. The test was carried out at a room temperature of 25 °C.

2.7 Statistical analysis

Statistical analyses were performed using R software version 3.3.3 (R Core Team (2017)).

3. Results and discussion

3.1 Structural changes in the cell wall and cell membrane after freeze-thawing

Figure 3 shows microscopic images of the apple flesh tissue before and after freeze-thawing. In the nonfrozen tissue, round shape cells 300 to 500 μm in diameter were densely arranged and small intercellular spaces were observed (Fig. 3a). However, in the frozen-thawed sample tissue shown in Fig. 3b, the intercellular spaces were greatly expanded to the large indefinite shape spaces approximately 500 to 1000 μm in length, and cells were markedly shrunk. This phenomenon is thought to result from the dehydration of intracellular fluid accompanied with the growth of ice crystals formed in the extracellular area. Because of this ice crystal formation process, the original cell wall structure was destroyed, leaving large spaces as previously reported by Chassagne-Berces et al. (2009).

The parameters of the equivalent circuit model (b) in Fig. 2, estimated from the electrical impedance characteristics, are shown in Table 1. The values of R^2 in the model fitting were over 0.999 and 0.998 for nonfrozen and frozen-thawed samples, respectively, indicating that the model is suitable to describe the impedance characteristics of the samples. During a freeze-thaw cycle, cells are subjected to a multitude of stresses including chilling stress, and mechanical and chemical stresses resulting from ice crystal formation (Steponkus, 1984). It has been demonstrated that ion leakage in cell membrane occurs prior to freezing injury (Palta, 1990), suggesting that the loss of osmotic responsiveness of plant cells may be due to low-temperature-induced alterations in the plasma membrane structure (Marangoni et al., 1996). The decrease in the extracellular fluid resistance, R_e, and increase in the intracellular fluid

282 resistance, R_i, shown in Table 1 could be explained by the changes in the intra- and
283 extracellular electrolyte concentrations, caused by the leakage of the intracellular fluid
284 to the extracellular region resulted from the cell membrane damage during freezing-
285 thawing process.

286 The cell membrane capacitance, C_m, decreased after freeze-thawing. The same
287 phenomenon has been reported for potatoes (Imaizumi et al., 2015; Zhang et al., 1993)
288 and spinach (Watanabe et al., 2017) during heating. The high C_m value of the fresh
289 tissue is thought to be attributable to the lipid bilayer structure of the membrane
290 (Ashrafuzzaman and Tuszynski, 2013); therefore, the decrease in C_m of the frozen-
291 thawed sample observed in this study is suggested to be a result of the structural
292 destruction of the cell membrane due to ice crystal formation during freezing.

293

294 *3.2 Effect of prefreezing on the drying rate of apple samples*

295 Figure 4a shows the changes in the moisture content versus drying time for the
296 nontreated and prefrozen-thawed samples during AD. For both samples, the moisture
297 content decreased faster at higher drying temperatures. Compared to the nontreated
298 sample, the drying of prefrozen samples progressed rapidly, even at the same drying
299 temperature. As with AD, prefrozen samples dried faster than nontreated samples during
300 MVD (Fig. 4b). At the beginning of the MVD process, the initial moisture content of
301 the prefrozen sample declined because the internal moisture was squeezed from the
302 damaged tissue when the pressure was reduced to the target value of 1.5 kPa.

303 Solid and dashed lines in the figure represent the least squares regression

analysis of the exponential model (Eq. 1). The correlation coefficient showed a good fit with the experimental data ($0.996 \leq R^2$), indicating that the model is appropriate for characterizing the changes in the moisture content of apples during drying. The drying rate constant k values estimated from the analysis are shown in Table 2. Although the values of k of MVD cannot be compared with those of AD under the same temperature condition, the values tended to be higher by roughly 3 to 4 times than those of AD. The higher drying rate in MVD was attributed to the promotion of moisture transfer from the interior of the drying sample to the surface, due to the microwave irradiation that penetrates the sample interior and selectively acts on the contained water molecules. The prefrozen sample showed approximately 1.2 to 1.3 times higher values of k compared to those of nontreated samples in both AD and MVD. As mentioned previously, the cell wall structure and cell membrane were damaged by ice crystal formation during freezing. Therefore, it was proposed that the increased drying rate of prefrozen samples was due to the accelerated water permeability of the sample tissue following the structural collapse of the cell wall and membrane, as reported by Alvarez et al. (1995), who claimed that the disruption of membranes and degradation of the middle lamella and hemicellulosic polysaccharides present in the cell wall enhanced moisture diffusivity in the plant tissue during air drying. In terms of cell membranes, the previous study in which the impedance characteristics of the potato tissue was monitored during drying has revealed that the cell membranes were gradually damaged from the initial moisture content to 1.0 (dry basis) suggesting that the water permeability in the tissue increased even during drying (Ando et al., 2014). In this study,

however, high water permeability was maintained throughout the drying process by preliminarily destroying the cell membrane, leading to higher drying rate. Especially in MVD, the drying time required was reduced by about half at each microwave power condition due to the decreased initial moisture content, resulting from the reduced pressure treatment and increased drying rate.

Figure 5 shows changes in the temperature of the center part of the samples until the end of drying. In the AD sample, temperature elevations of the prefrozen samples tended to be suppressed compared to the nonfrozen samples at each drying temperature (Fig. 5a); this was because the applied heat was more efficiently utilized by the phase change (evaporation) of water at a high rate of drying in the prefrozen samples. In the MVD of nonfrozen samples, the center temperature was gradually increased to approximately 70 °C at each drying temperature, by utilizing temperature cycling in the irradiation-pause cycle of the microwave (Fig. 5b). In the MVD, the boiling point of the sample was increased even in the reduced pressure because the sample moisture was concentrated as drying proceeded. Also, the supplied microwave energy per moisture amount was increased as the moisture decreased during drying. In addition to these conditions, drying rate of the nonfrozen sample was low especially in the end of drying, therefore, temperature was not suppressed and kept increasing. The temperature of the prefrozen MVD sample decreased from initial temperature of 25 °C to about 20 °C at first 0.5 h because of the decreased boiling point in the reduced pressure environment and the efficient absorption of latent heat due to the high drying rate of the prefrozen sample. The temperature maintained below 40 °C until end of the

348 drying at each microwave power condition while the temperature of the nontreated
349 sample was not suppressed because of the low water evaporation rate during drying.
350 The result indicates that applied microwave energy was spend more effectively for
351 water evaporation in the prefrozen MVD sample.
352
353 *3.3 Effects of prefreezing on the structural and mechanical properties of dried*
354 *samples*
355 Figure 6 shows the reconstructed images and tomograms of the dried samples.
356 The prefrozen AD sample showed less shrinkage during drying compared to the
357 nonfrozen AD sample. In the nonfrozen AD sample (Fig. 6a), fine internal voids were
358 scattered throughout and a dense internal structure was observed; whereas a porous
359 internal structure with relatively larger voids, 200–400 μm in diameter, was observed in
360 the prefrozen AD sample (Fig. 6b). The shrinkage of prefrozen AD sample was
361 inhibited because the spaces formed by ice crystal formation during freezing (as shown
362 in Fig. 3b) functioned as a vent and the pressure difference between the inside and
363 surface of the sample tissue, which is a driving force of shrinkage during drying, was
364 mitigated.
365 In the nonfrozen MVD sample shown in Fig. 6c, the center part appeared to be
366 tightly compressed and formed a dense structure (white region in the image), while a
367 porous structure is observed in the surface region. In the microstructure image, both
368 dense and porous areas can be observed. Figure 7 shows the mechanism of the structural
369 formation of MVD samples. In the nonfrozen sample tissue, the expanded internal water

vapor generated under microwave irradiation, in which heating proceeds from the center of the sample, leaked slightly from the tissue through the intercellular gaps. During the following pause in microwave irradiation, the remaining gas within the tissue is cooled and attempts to return to its original volume. However, the amount of the gas was reduced because of the leakage during irradiation, and as a result, the sample volume shrunk because the pressure within the tissue became negative. The dense structure of the MVD nonfrozen samples was attributed to the repetition of this cycle.

Since the cell wall and membrane structures of the frozen-thawed tissue were damaged and characterized by high gas permeability, the generated gas during microwave heating is able to pass through the tissue at a higher rate than in the nonfrozen tissue. Even during the cooling phase, a high permeability was maintained, and therefore, the tissue showed less shrinkage due to the mitigation of pressure differences between the interior and exterior. As a result, the porous structure of the prefrozen MVD sample showed void diameters of 400–600 μm (Fig. 6d). The microwave puffing which is a rapid volume expansion of a sample at relatively low moisture content that occurs during microwave treatment (Zhen et al., 2013; Rakesh and Datta, 2011) was not observed in this study because the internal pressure required for the puffing was not generated as mentioned above, and also because the microwave power output was relatively low. The more porous structure of the prefrozen MVD sample compared to the prefrozen AD sample suggests that heating and moisture evaporation from the interior during microwave irradiation acted as a force radiating from the sample interior.

392 Typical puncture curves and mechanical parameters for the dried samples are
393 shown in Fig. 8 and Table 3, respectively. The high value of maximum stress σ_{max}
394 observed in the nonfrozen MVD samples was attributed to the densely compressed
395 nature of the sample, as shown in Fig. 6c. The puncture curve of the nonfrozen AD
396 sample showed a smooth shape, and the sample showed a significantly lower E value,
397 which is used as a measure of stiffness, despite the almost identical value of σ_{max} as the
398 prefrozen AD sample. The similar shape of the puncture curves with many peaks
399 observed in the prefrozen AD and MVD samples could originate from the porous
400 internal structure containing many separate compartments. The prefrozen MVD sample
401 showed a smaller σ_{max} value and about twice the number of peaks compared to the
402 prefrozen AD sample. Dogan and Kokini (2007) reported that the number of peaks was
403 correlated with sensory crispness in an experiment using corn extrudates. Therefore, the
404 higher number of peaks in the prefrozen MVD sample indicates that the sample is
405 crisper than the prefrozen AD sample, and it is suggested that the softer and crisper
406 property of the prefrozen MVD sample is due to its brittle structure with larger internal
407 voids.
408
409 **4. Conclusions**
410
411 The findings obtained from the present study, i.e., the relation of the drying rate
412 and the cellular damage, and the mechanism of structural formation during MVD can be
413 valuable in effectively manufacturing dried foods with a unique texture. Evaluation of

414 production energy costs and quality, such as flavor or nutrient components, and
415 development of a recovery and recycling technique for drip discharged from the sample
416 under reduced pressure should be addressed as future works. In addition, the suitable
417 prefreezing conditions (e.g., temperature and time) should be investigated to maximize
418 the drying rate and energy efficiency for industrial application.
419
420 **Acknowledgement**
421
422 This study was supported by a research grant of the Society of Agricultural
423 Structures, Japan.
424
425 **References**
426
427 Abano, E. E., Ma, H., & Qu, W. (2012). Influence of combined microwave-vacuum
428 drying on drying kinetics and quality of dried tomato slices. *Journal of Food*
429 *Quality*, *35*, 159–168.
430 Alvarez, C. A., Aguerre, R., Gómez, R., Vidales, S., Alzamora, S. M., & Gerschenson,
431 L. N. (1995). Air dehydration of strawberries: Effects of blanching and osmotic
432 pretreatments on the kinetics of moisture transport. Journal of Food Engineering,
433 *25*(2), 167–178.
434 Ando, Y., Mizutani, K., & Wakatsuki, N. (2014). Electrical impedance analysis of potato
435 tissues during drying. *Journal of Food Engineering, 121*, 24–31.

436 Ando, Y., Maeda, Y., Mizutani, K., Wakatsuki, N., Hagiwara, S., & Nabetani, H. (2016).
437 Impact of blanching and freeze-thaw pretreatment on drying rate of carrot roots
438 in relation to changes in cell membrane function and cell wall structure. *LWT -*
439 *Food Science and Technology*, *71*, 40–46.
440 Ando, Y., Hagiwara, S., & Nabetani, H. (2017). Thermal inactivation kinetics of pectin
441 methylesterase and the impact of thermal treatment on the texture, electrical
442 impedance characteristics and cell wall structure of Japanese radish (*Raphanus*
443 *sativus* L.). *Journal of Food Engineering, 199*, 9–18.
444 Ashrafuzzaman, M., & Tuszynski, J. A. (2013). Structure of membranes. In *Membrane*
445 *Biophysics* (pp.9–30). Springer-Verlag Berlin Heidelberg.
446 Bondaruk, J., Markowski, M., & Błaszczak, W. (2007). Effect of drying conditions on
447 the quality of vacuum-microwave dried potato cubes. *Journal of Food*
448 *Engineering*, *81*, 306–312.
449 Babalis, S. J., Papanicolaou, E., Kyriakis, N., & Belessiotis, V. G. (2006). Evaluation of
450 thin-layer drying models for describing drying kinetics of figs (*Ficus carica*).
451 *Journal of Food Engineering, 75*(2), 205–214.
452 Bai-Ngew, S., Therdthai, N., & Dhamvithee, P. (2011). Characterization of microwave
453 vacuum-dried durian chips. *Journal of Food Engineering*, *104*, 114–122.
454 Chassagne-Berces, S., Poirier, C., Devaux, M., Fonseca, F., Lahaye, M., Pigorini, G.,
455 Girault, C., Marin, M., & Guillon, F. (2009). Changes in texture, cellular
456 structure and cell wall composition in apple tissue as a result of freezing. *Food*
457 *Research International*, *42*(7), 788–797.

458 Chong, C. H., Figiel, A., Law, C. L., & Wojdyło, A. (2014). Combined drying of apple
459 cubes by using of heat pump, vacuum-microwave, and intermittent techniques.
460 *Food and Bioprocess Technology*, *7*, 975–989.
461 Cui, Z., Xu, S., & Sun, D. (2004). Microwave–vacuum drying kinetics of carrot slices.
462 *Journal of Food Engineering*, *65*, 157–164.
463 Cui, Z., Xu, S., & Sun, D. (2004). Effect of microwave-vacuum drying on the
464 carotenoids retention of carrot slices and chlorophyll retention of Chinese chive
465 leaves. *Drying Technology*, *22* (3), 563–575.
466 Dandamrongrak, R., Young, G., & Mason, R. (2002). Evaluation of various pre-
467 treatments for the dehydration of banana and selection of suitable drying models.
468 *Journal of Food Engineering, 55*(2), 139–146.
469 Dogan, H., & Kokini, J. L. (2007). Psychophysical markers for crispness and influence
470 of phase behavior and structure. *Journal of Texture Studies*, *38*, 324–354.
471 Drouzas, A. E., & Schubert, H. (1996). Microwave application in vacuum drying of
472 fruits. *Journal of Food Engineering*, *28*, 203–209.
473 Durance, T. D., & Wang, J. H. (2002). Energy consumption, density, and rehydration
474 rate of vacuum microwave- and hot-air convection- dehydrated tomatoes.
475 *Journal of Food Science*, *67* (6), 2212–2216.
476 Eshtiaghi, M. N., Stute, R., & Knorr, D. (1994). High-pressure and freezing
477 pretreatment effects on drying, rehydration, texture and color of green beans,
478 carrots and potatoes. *Journal of Food Science, 59*(6), 1168–1170.
479 Giri, S. K., & Prasad, S. (2007). Drying kinetics and rehydration characteristics of

480 microwave-vacuum and convective hot-air dried mushrooms. *Journal of Food*
481 *Engineering*, *78*, 512–521.
482 Hsu, C. H., & Mansfeld, F. (2001). Technical note: Concerning the conversion of the
483 constant phase element parameter Y-0 into a capacitance. *Corrosion, 57*(9),
484 747–748.
485 Hu, Q., Zhang, M., Mujumdar, A. S., Xiao, G., & Sun, J. (2006). Drying of edamames
486 by hot air and vacuum microwave combination. *Journal of Food Engineering*,
487 *77*, 977–982.
488 Huang, L., Zhang, M., Wang, L., Mujumdar, A. S., & Sun, D. (2012). Influence of
489 combination drying method on composition, texture, aroma and microstructure
490 of apple slices. *LWT - Food Science and Technology*, *47*, 183–188.
491 Imaizumi, T., Tanaka, F., Hamanaka, D., Sato, Y, & Uchino, T. (2015). Effects of hot
492 water treatment on electrical properties, cell membrane structure and texture of
493 potato tubers. *Journal of Food Engineering*, *162*, 56–62.
494 Jiang, H., Zhang, M., Mujumdar, A. S., & Lim, R. (2014). Comparison of drying
495 characteristic and uniformity of banana cubes dried by pulse-spouted microwave
496 vacuum drying, freeze drying and microwave freeze drying. *Journal of the*
497 *Science of Food and Agriculture*, *94*, 1827–1834.
498 Jiang, N., Liu, C., Li, D., Zhang, Z., Liu, C., Wang, D., Niu, L., & Zhang, M. (2017).
499 Evaluation of freeze drying combined with microwave vacuum drying for
500 functional okra snacks: Antioxidant properties, sensory quality, and energy
501 consumption. *LWT - Food Science and Technology*, *82*, 216–226.

Lin, T. M., Durance, D., & Scaman, C. H. (1998). Characterization of vacuum microwave, air and freeze dried carrot slices. *Food Research International*, *31* (2), 111–117.

Macdonald, J. R. (1992). Impedance spectroscopy. *Annals of Biomedical Engineering, 20*(3), 289–305.

Marangoni, A. G., Palma, T., & Stanley, D. W. (1996). Membrane effects in postharvest physiology. Postharvest Biology and Technology, *7*(3), 193–217.

Nahimana, H., & Zhang, M. (2011). Shrinkage and color change during microwave vacuum drying of carrot. *Drying Technology*, *29*, 836–847.

Nieto, A., Salvatori, D., Castro, M. A., & Alzamora, S. M. (1998). Air drying behaviour of apples as affected by blanching and glucose impregnation. *Journal of Food Engineering, 36*(1), 63–79.

Orikasa, T., Wu, L., Shiina, T., & Tagawa, A. (2008). Drying characteristics of kiwifruit during hot air drying. *Journal of Food Engineering, 85*(2), 303–308.

Orikasa, T., Koide, S., Sugawara, H., Yoshida, M., Kato, K., Matsushima, U., Okada, M., Watanabe, T., Ando, Y., Shiina, T., & Tagawa, A. (2018). Applicability of vacuum-microwave drying for tomato fruit based on evaluations of energy cost, color, functional components and sensory qualities. *Journal of Food Processing and Preservation*, https://doi.org/10.1111/jfpp.13625.

Palta, J. P. (1990). Stress interactions at the cellular and membrane levels. *HortScience*, *25*(11), 1377–1381.

Pu, Y. & Sun, D. (2015). Vis-NIR hyperspectral imaging in visualizing moisture

524 distribution of mango slices during microwave-vacuum drying. *Food Chemistry*,
525 *188*, 271–278.
526 Rakesh, V., & Datta, A. (2011). Microwave puffing: Determination of optimal
527 conditions using a coupled multiphase porous media - Large deformation model.
528 *Journal of Food Engineering*, *107*, 152–163.
529 Sagar, V. R., & Suresh, K. P. (2010). Recent advances in drying and dehydration of
530 fruits and vegetables: a review. *Journal of Food Science and Technology*, *47*(1),
531 15–26.
532 Stępień, B. (2008). Effect of vacuum-microwave drying on selected mechanical and
533 rheological properties of carrot. *Biosystems Engineering*, *99*, 234–238.
534 Steponkus, P. L. (1984). Role of the plasma membrane in freezing injury and cold
535 acclimation. *Ann. Rev. Plant Physiol.*, *35*, 543–584.
536 The Council for Science and Technology, MEXT, Japan (2005). Analytical manual for
537 standard tables of food composition in Japan (5th revised and enlarged ed., pp.
538 1-40). National Printing Bureau, Tokyo. (in Japanese)
539 Therdthai, N., & Zhou, W. (2009). Characterization of microwave vacuum drying and
540 hot air drying of mint leaves (*Mentha cordifolia* Opiz ex Fresen), *Journal of*
541 *Food Engineering*, *91*, 482–489.
542 Vaccarezza, L. M., Lombardi, J. L., & Chirife, J. (1974). Kinetics of moisture
543 movement during air drying of sugar beet root. *International Journal of Food*
544 *Science & Technology, 9*(3), 317–327.
545 Watanabe, T., Ando, Y., Orikasa, T., Shiina, T., & Kohyama, K. (2017). Effect of short

546 time heating on the mechanical fracture and electrical impedance properties of
547 spinach (*Spinacia oleracea* L.). *Journal of Food Engineering, 194,* 9–14.
548 Yanyang, X., Min, Z., Mujumdar, A. S., Le-qun, Z., & Jin-cai, S. (2004). Studies on hot
549 air and microwave vacuum drying of wild cabbage. *Drying Technology*, *22* (9),
550 2201–2209.
551 Yongsawatdigul, J., & Gunasekaran, S. (1996). Microwave-vacuum drying of
552 cranberries: Part I. Energy use and efficiency. *Journal of Food Processing and*
553 *Preservation*, *20*, 121–143.
554 Zhang, M. I. N., & Willison, J. H. M. (1992a). Electrical impedance analysis in plant
555 tissues: i*n vivo* detection of freezing injury. *Canadian Journal of Botany, 70*(11),
556 2254–2258.
557 Zhang, M. I. N., & Willison, J. H. M. (1992b). Electrical impedance analysis in plant
558 tissues: The effect of freeze thaw injury on the electrical properties of potato
559 tuber and carrot root tissues. *Canadian Journal of Plant Science, 72*(2),
560 545–553.
561 Zhang, M. I. N., Willison, J. H. M., Cox, M. A., & Hall, S. A. (1993). Measurement of
562 heat injury in plant tissue by using electrical impedance analysis. *Canadian*
563 *Journal of Botany, 71*(12), 1605–1611.
564 Zheng, X., Liu, C., Shi, J., Xue, S., Mu, Y., Lin, Z., & Liu, H. (2013). Analysis of
565 volume expansion and dehydration rate of berry slab under microwave-vacuum
566 puffing conditions, *LWT - Food Science and Technology*, *52*, 39–48.
567 Zielinska, M., & Markowski, M. (2016). The influence of microwave-assisted drying

techniques on the rehydration behavior of blueberries (*Vaccinium corymbosum* L.). *Food Chemistry*, *196*, 1188–1196.

Zielinska, M., & Michalska, A. (2016). Microwave-assisted drying of blueberry (*Vaccinium corymbosum* L.) fruits: Drying kinetics, polyphenols, anthocyanins, antioxidant capacity, colour and texture. *Food Chemistry*, *212*, 671–680.

Zielinska, M., Ropelewska, E., & Markowski, M. (2017). Thermophysical properties of raw, hot-air and microwave-vacuum dried cranberry fruits (*Vaccinium macrocarpon*). *LWT - Food Science and Technology*, *85*, 204–211.

Zielinska, M., Sadowski, P., & Błaszczak, W. (2015). Freezing/thawing and microwave-assisted drying of blueberries (*Vaccinium corymbosum* L.). *LWT - Food Science and Technology*, *62*(1, part 2), 555–563.

Zielinska, M., Zielinska, D., & Markowski, M. (2018). The effect of microwave-vacuum pretreatment on the drying kinetics, color and the content of bioactive compounds in osmo-microwave-vacuum dried cranberries (*Vaccinium macrocarpon*). *Food and Bioprocess Technology*, *11*(3), 585–602.

Figure 1

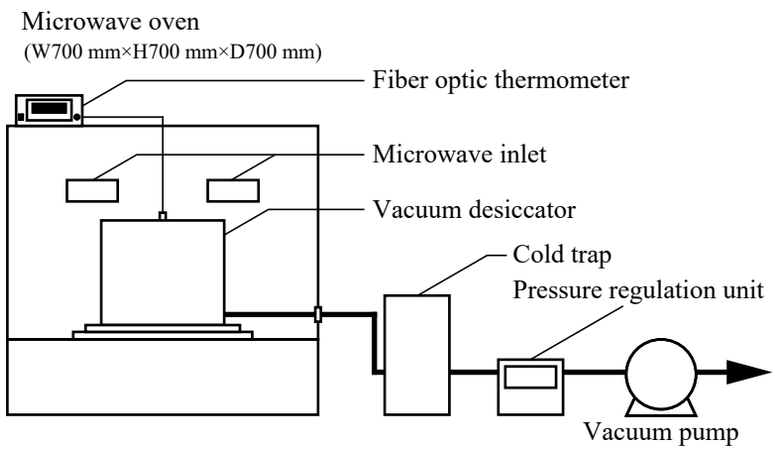
Microwave oven
(W700 mm×H700 mm×D700 mm)
Fiber optic thermometer
Microwave inlet
Vacuum desiccator
Cold trap
Pressure regulation unit
Vacuum pump

Figure 2

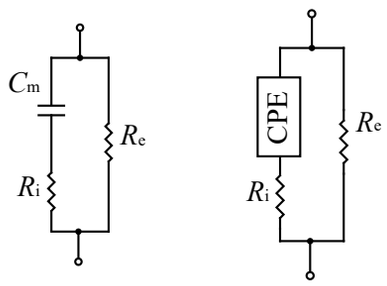

(a) (b)

Figure 3

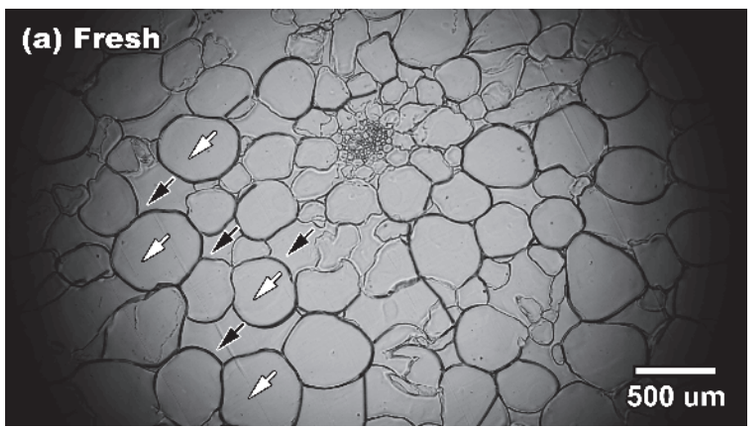

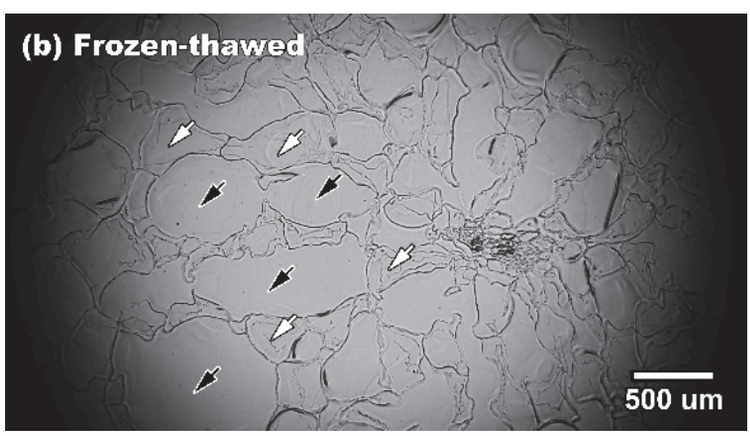

Figure 4

(a) Air drying

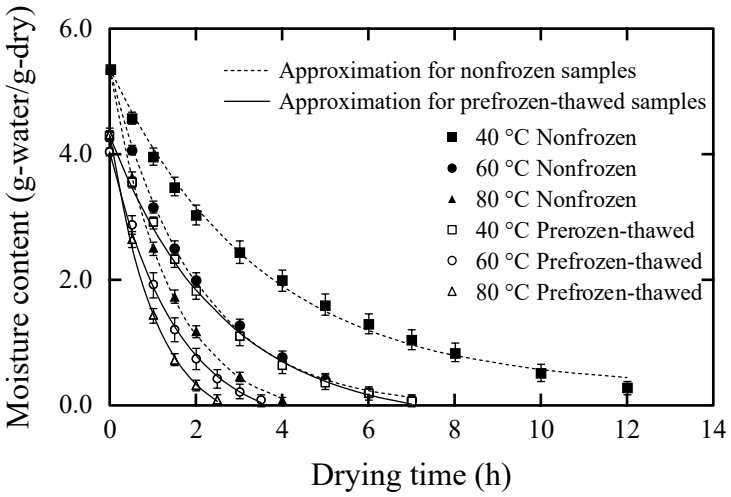

(b) Microwave-vacuum drying

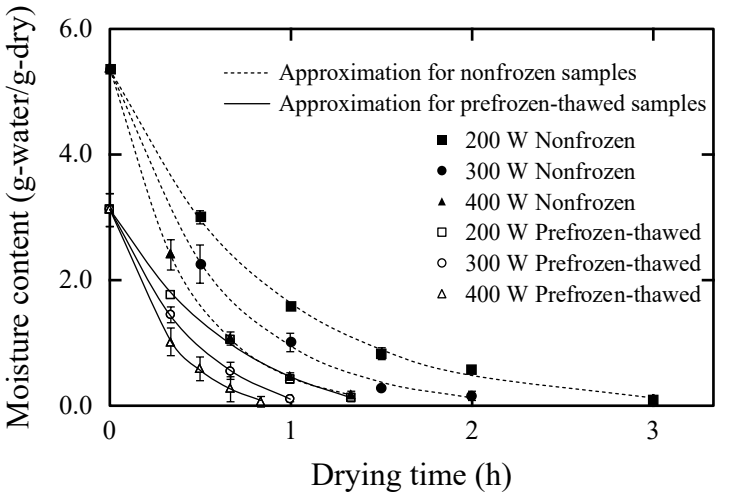

Figure 5

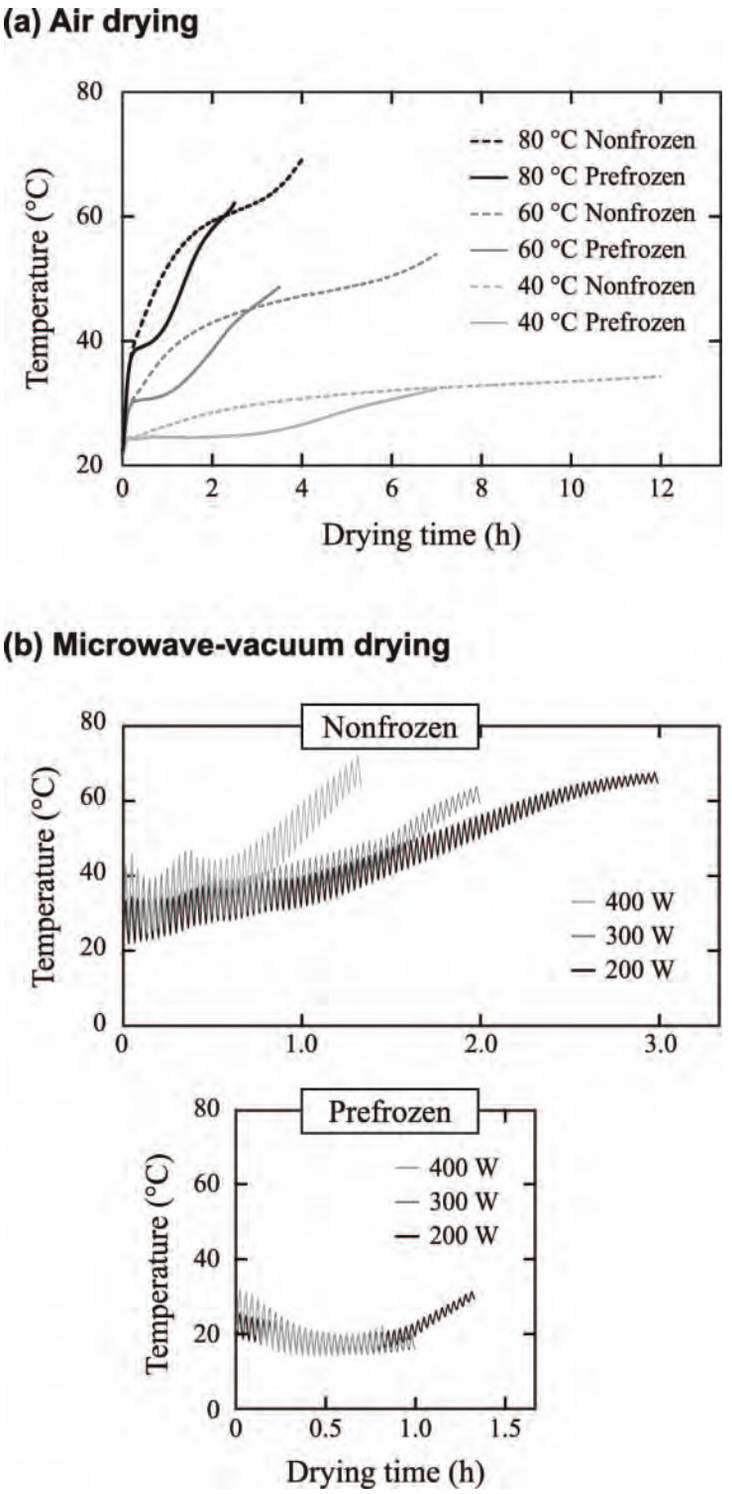
(a) Air drying
Temperature (°C)
Drying time (h)
80 °C Nonfrozen
80 °C Prefrozen
60 °C Nonfrozen
60 °C Prefrozen
40 °C Nonfrozen
40 °C Prefrozen
(b) Microwave-vacuum drying
Nonfrozen
400 W
300 W
200 W
Prefrozen
400 W
300 W
200 W
Temperature (°C)
Drying time (h)

Figure 6

(a) AD - not treated

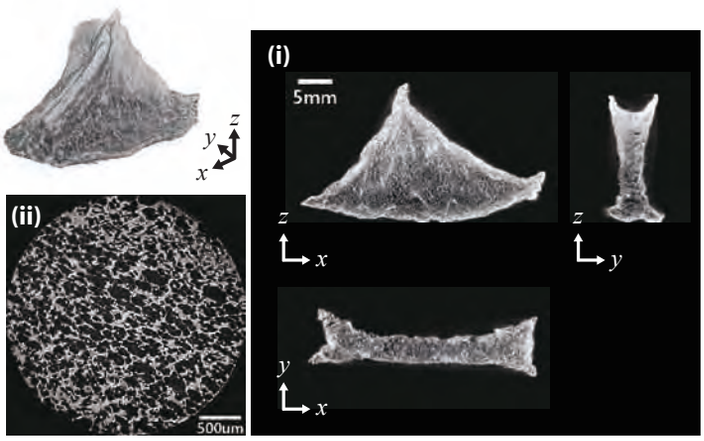

(b) AD - prefrozen

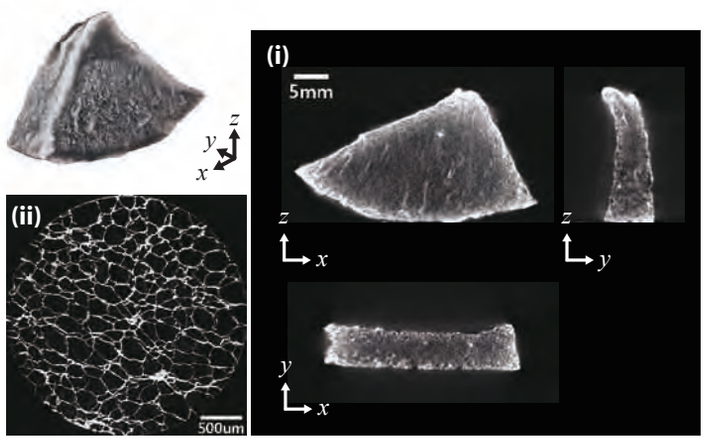

(c) MVD - not treated

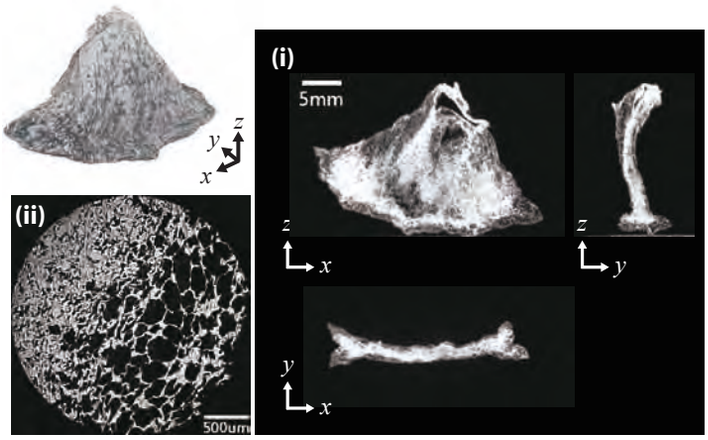

(d) MVD - prefrozen

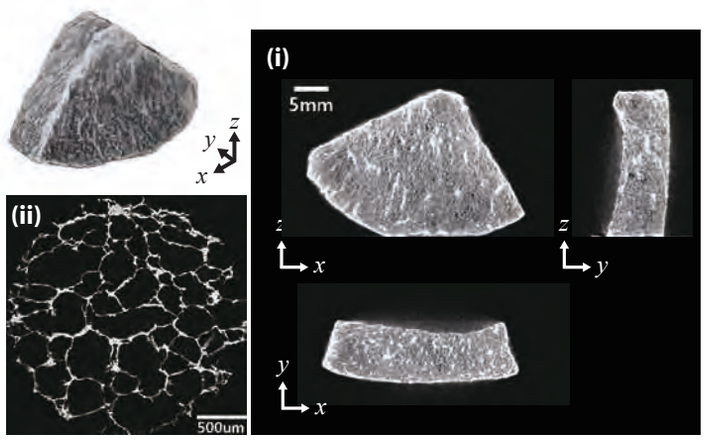

Figure 7

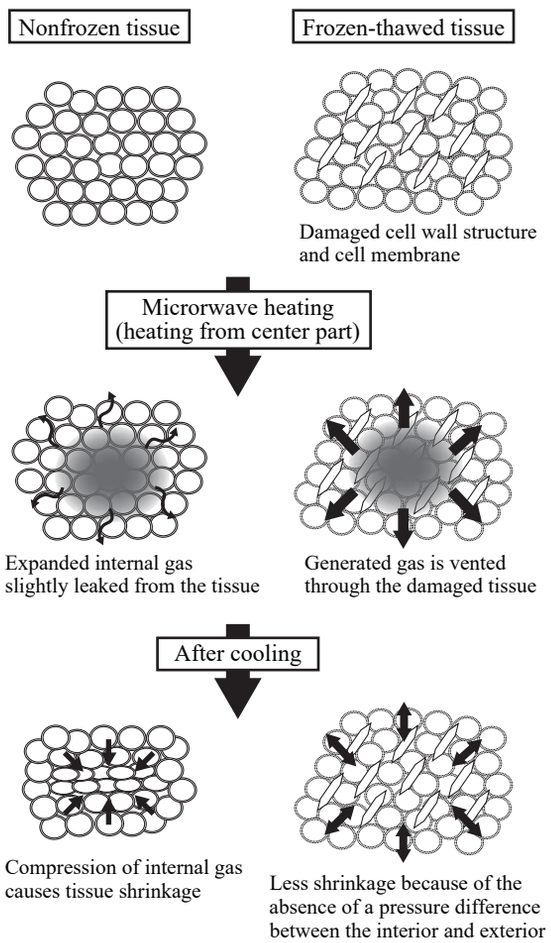
Nonfrozen tissue
Frozen-thawed tissue
Damaged cell wall structure
and cell membrane
Microrwave heating
(heating from center part)
Expanded internal gas
slightly leaked from the tissue
Generated gas is vented
through the damaged tissue
After cooling
Compression of internal gas
causes tissue shrinkage
Less shrinkage because of the
absence of a pressure difference
between the interior and exterior

Figure 8

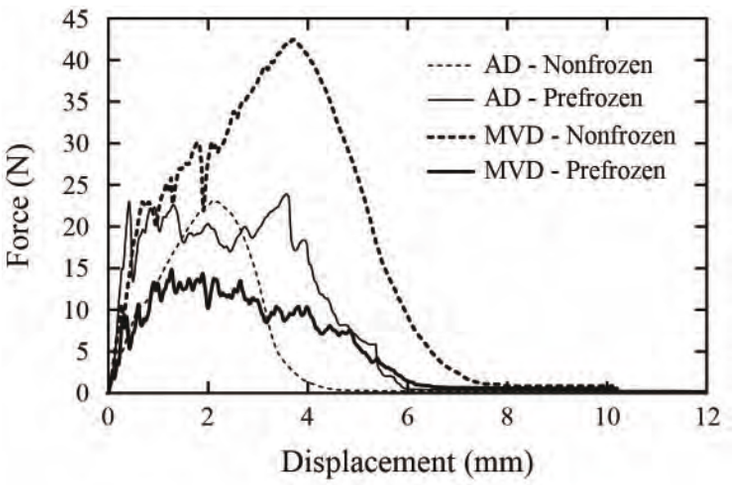
45
40
35
30
25
20
15
10
5
0
Force (N)
0
2
4
6
8
10
12
Displacement (mm)
AD - Nonfrozen
AD - Prefrozen
MVD - Nonfrozen
MVD - Prefrozen

Figure captions

Fig. 1. Schematic diagram of the apparatus for microwave-vacuum drying.

Fig. 2. Equivalent circuit models for biological tissues: model for single cell (a), and model for electrically inhomogeneous multiple cells with a time constant distribution (b). C_m: capacitance of cell membrane, R_i: intracellular fluid resistance, R_e: extracellular fluid resistance, CPE: constant phase element.

Fig. 3. Microscopic images of fresh (a) and frozen-thawed (b) apple flesh tissue sections. White arrows represent cells and black arrows represent intercellular spaces.

Fig. 4. Changes in the moisture content of apple samples during drying. The data are mean values of 3–4 replicates. Bars denote standard deviation. Solid and dashed lines represent the least squares regression analysis of the first-order reaction equation (Eq. 1).

Fig. 5. Changes in temperature of the central part of apple samples during drying. The data are mean values of 3–4 replicates.

Fig. 6. Reconstructed images and tomograms of the dried apple samples. AD: air dried sample at 60 °C, MVD: microwave-vacuum dried sample at a power of 300 W. (i) Whole image of the dried sample, (ii) microstructural image of the center part of the dried sample.

Fig. 7. Mechanism of the structural formation of dried apple samples during microwave-vacuum drying.

Fig. 8. Typical puncture curves of the dried apple samples. AD: air dried sample at 60 °C, MVD: microwave-vacuum dried sample at a power of 300 W.

Table 1 Equivalent circuit parameters obtained from the model fitting.

	C_m (nF)	R_e (kΩ)	R_i (kΩ)	R^2
Nonfrozen	$1.64^{a} \pm 0.08$	$41.4^{a} \pm 4.5$	$3.60^{a} \pm 0.34$	≥ 0.999
Frozen-thawed	$0.41^{b} \pm 0.07$	$3.8^{b} \pm 0.6$	$6.27^{b} \pm 0.84$	≥ 0.998

C_m: capacitance of cell membrane, R_e: extracellular fluid resistance, R_i: intracellular fluid resistance, R^2: determination coefficient in the model fitting. The values of C_m, R_e and R_i represent the mean values of 16 replicates (± standard deviation). Different superscripts indicate significant differences ($p < 0.01$) between the means in the same column compared by a *t*-test.

Table 2 Drying rate constant k (h^{-1}) estimated from the exponential model for dried samples (Eq.1).

		Nonfrozen	Prefrozen
AD	40 °C	0.285	0.382
	60 °C	0.494	0.656
	80 °C	0.709	0.922
MVD	200 W	1.171	1.372
	300 W	1.674	1.945
	400 W	2.357	2.951

AD: air drying, MVD: microwave-vacuum drying.

Table 3 Mechanical parameters of the dried apple samples determined using the puncture test.

	Thickness (mm)	Maximum stress σ_{max} (Pa)	Elastic modulus E (Pa)	Number of peaks (–)
AD - Nonfrozen	$3.18^{c} \pm 0.37$	$29968^{b} \pm 3276$	$36886^{c} \pm 4752$	–
AD - Prefrozen	$5.63^{b} \pm 0.55$	$24913^{bc} \pm 5653$	$260945^{a} \pm 100959$	$21.27^{b} \pm 7.23$
MVD - Nonfrozen	$3.25^{c} \pm 0.44$	$55158^{a} \pm 10997$	$140633^{b} \pm 44150$	–
MVD - Prefrozen	$6.33^{a} \pm 0.62$	$18941^{c} \pm 8075$	$195112^{ab} \pm 10574$	$42.13^{a} \pm 7.37$

AD: air dried at 60 °C, MVD: microwave-vacuum dried at 300 W. The values represent the mean values of 16–18 replicates (± standard deviation). Different superscripts indicate significant differences ($p < 0.05$) between the means in the same column compared by a Tukey’ s multiple range test.